Properties of Hartree-Fock solutions of the three-dimensional electron gas

L. Baguet,[1] F. Delyon,[2] B. Bernu,[1] and M. Holzmann[1,3]

[1] *LPTMC, UMR 7600 of CNRS, Université P. et M. Curie, Paris, France*
[2] *CPHT, UMR 7644 of CNRS, École Polytechnique, Palaiseau, France*
[3] *Univ. Grenoble Alpes, LPMMC, F-38000 Grenoble, France*
CNRS, LPMMC, F- 38000 Grenoble, France

(Dated: October 27, 2014)

In a previous letter, L. Baguet et al., (Phys. Rev. Lett. **111**, 166402 (2013)), we presented the ground state phase diagram of the homogeneous electron gas in three dimensions within the Hartree-Fock approximation yielding incommensurate crystal states at high density. Here, we analyze the properties of these solutions. In particular, at high density we find universal behavior of the incommensurate crystal strongly supporting the existence of a spin density wave ground state.

PACS numbers: 71.10.-w, 71.10.Ca, 71.10.Hf, 71.30.+h, 03.67.Ac

arXiv:1404.7652v3 [cond-mat.str-el] 23 Oct 2014

I. INTRODUCTION

Most solid properties depend on the electron behavior, and one of the fundamental issues in solid state physics is the understanding of how electrons roam in crystals. Within the independent particle approximation, electronic properties are studied considering a model where electrons interact only with the positive ions of the crystal, but each electron remains independent of the others. Within this picture, insulators are characterized by completely filled bands, otherwise the state is metallic. The failure of band theory to predict insulating behavior and the role played by correlations due to electron-electron interaction has been subject to intense research starting from the early work of Mott[1].

In the limit where the positive charge of the ions in the crystal is smeared out uniformly through the whole system, electronic correlations are separated from crystal field effects. In this so called jellium model of a solid, the electrons interact with each others via the Coulomb interaction ($\sim 1/r$) and global electroneutrality is insured by a uniform positive charge background. Despite its simplicity, this model is directly relevant in a few cases, for example solid sodium[2].

The Hartree-Fock (HF) approximation where electron-electron interactions are replaced by a simple self-consistent field provides a first step to go beyond the independent electron approximation[3]. However, the resulting Hartree-Fock equations are non-local and non-linear. Even for the homogeneous electron gas model, the quantitative determination of the ground state phase diagram – which depends only on density – has been a challenging task[4–8]; large part of the HF phase diagram in three dimensions has been established only recently[9].

Two possible phases of jellium have been widely investigated: the Fermi Gas (FG), where electrons are completely delocalized and form a uniform negative charge distribution, and the Wigner crystal (WC) where electrons are organized on a lattice. At high densities the kinetic energy dominates so the FG is believed to be the ground state, and for low densities, the long-range interaction makes electrons form the WC.

However, already Wigner argued that the unpolarized FG is unstable even for high densities[10]. Later, Overhauser[11] showed the instability of the unpolarized FG with respect to spin-density waves (SDW) within HF.

In Ref.[9], we have established the ground state phase diagram considering periodic states, which, besides the WC, also include the possibility of incommensurate crystals (IC) where the number of maxima in the charge (or spin) density is larger than the number of electrons. At high density these calculations confirmed the FG instability with respect to IC. In this paper, we provide a more complete description of both the method and the results. In particular, we focus on the physical properties of the HF states and on the universality of the results at high density giving further evidence for the SDW character of the high density ground state.

The paper is organized as follows. In Sec.II, we describe the model and introduce the basic definitions. Some technical aspects on its numerical solutions are given in Sec.III. The discussion of the results is presented in Sec.IV with our conclusions in Sec.V.

II. THE MODEL

We consider a periodic system, with N electrons of mass m_e in a three dimensional box of volume V, embedded in an homogeneous background of opposite charge with a density $N/V = 3/(4\pi a_B^3 r_s^3)$ where a_B is the Bohr radius. The Hamiltonian reads:

$$H = -\frac{\hbar^2}{2m_e}\sum_i \Delta_i + \frac{1}{V}\sum_{\mathbf{k}\neq 0} v_{\mathbf{k}} \sum_{i<j} e^{i\mathbf{k}.\mathbf{r}_{ij}} \qquad (1)$$

where $v_{\mathbf{k}} = 4\pi/\|\mathbf{k}\|^2$.

Hartree-Fock solutions are exterior products (Slater determinants) of single particle states ϕ_α denoted as $|\Psi\rangle = \bigwedge_{\alpha\in S} |\phi_\alpha\rangle$. In terms of density matrix, the Hartree-Fock solutions can be defined by a 1-body density matrix ρ_1 such that $\mathbf{Tr}\ \rho_1 = 1$ and $0 \leq \rho_1 \leq 1/N$,

that is all eigenvalues are in $[0, 1/N]$[12]. The two-body density matrix ρ_2 satisfies:

$$\rho_2(\underline{1},\underline{2};\underline{1}',\underline{2}') = \rho_1(\underline{1};\underline{1}')\rho_1(\underline{2};\underline{2}') - \rho_1(\underline{1};\underline{2}')\rho_1(\underline{2};\underline{1}'). \quad (2)$$

Now we restrict our study to periodic states: let Λ^* be a lattice generated by $\mathbf{L}_1, \mathbf{L}_2$ and $\mathbf{L}_3$, and $\rho_1(\mathbf{r}+\mathbf{L}_i, \mathbf{r}'+\mathbf{L}_i) = \rho_1(\mathbf{r},\mathbf{r}')$.

The reciprocal lattice Λ is generated by $\mathbf{Q}_1, \mathbf{Q}_2$ and $\mathbf{Q}_3$ such as $\mathbf{L}_i.\mathbf{Q}_j = 2\pi\delta_{ij}$ and we note $\mathcal{B}$ its Brillouin zone. Then

$$\rho_1 = \bigoplus_{\mathbf{k}\in\mathcal{B}} \rho_{\mathbf{k}} \quad (3)$$

where $\rho_{\mathbf{k}}$ are positive matrices satisfying $0 \le \rho_{\mathbf{k}} \le 1/N$. The simulation box is a parallelepiped generated from the vectors $M\mathbf{L}_i$, where M is some integer. So $V \sim M^3$, and the number of $\rho_{\mathbf{k}}$ is M^3. The thermodynamic limit is recovered for $M \to \infty$. The total energy per electron in Hartree unit reads:

$$e = \sum_{\mathbf{k}\in\mathcal{B}} \mathbf{Tr}\left(K_{\mathbf{k}} + \mathcal{V}_{\mathbf{k}}\right)\rho_{\mathbf{k}} \quad (4)$$

$$K_{\mathbf{k}}(\mathbf{q},\sigma;\mathbf{q}',\sigma') = \frac{a_B^2}{2}\|\mathbf{k}+\mathbf{q}\|^2\delta_{\mathbf{q}\mathbf{q}'}\delta_{\sigma\sigma'} \quad (5)$$

$$\mathcal{V}_{\mathbf{k}_1}(\mathbf{q}_1,\sigma_1;\mathbf{q}_1',\sigma_1') = \frac{2\pi a_B N}{V}\times$$
$$\Bigg[\delta_{\sigma_1\sigma_1'}\sum_{\mathbf{q}\in\Lambda}\frac{\delta_{\mathbf{q}_1'-(\mathbf{q}_1-\mathbf{q})}}{\|\mathbf{q}\|^2}\sum_{\substack{\mathbf{k}_2\in\mathcal{B}\\ \mathbf{q}_2\in\Lambda\\ \sigma}}\rho_{\mathbf{k}_2}(\mathbf{q}_2,\sigma;\mathbf{q}_2-\mathbf{q},\sigma) \quad (6)$$
$$-\sum_{\substack{\mathbf{k}_2\in\mathcal{B}\\ \mathbf{q},\mathbf{q}_2\in\Lambda}}\frac{\delta_{\mathbf{q}_1'-(\mathbf{q}_1-\mathbf{q})}}{\|\mathbf{k}_1+\mathbf{q}_1-\mathbf{k}_2-\mathbf{q}_2\|^2}\rho_{\mathbf{k}_2}(\mathbf{q}_2,\sigma_1;\mathbf{q}_2-\mathbf{q},\sigma_1')\Bigg]$$

with $\mathbf{Tr}A_{\mathbf{k}}\rho_{\mathbf{k}} = \sum_{\mathbf{q}\mathbf{q}'\in\Lambda,\sigma\sigma'} A_{\mathbf{k}}(\mathbf{q},\sigma;\mathbf{q}',\sigma')\rho_{\mathbf{k}}(\mathbf{q}',\sigma';\mathbf{q},\sigma)$.

In this paper, k_F denotes the Fermi wave vector depending on the gas polarization. We have

$$k_F a_B = \frac{\alpha}{r_s}, \qquad \alpha = \left(\frac{9\pi}{2n_s}\right)^{1/3} \quad (7)$$

where $n_s = 1$ for fully polarized gas (P) and $n_s = 2$ for the unpolarized gas (U). The one-body density matrices of the Fermi gas (FG) reads

$$\rho_{\mathbf{k}}(\mathbf{q},\mathbf{q}') = \frac{1}{N}\delta_{\mathbf{q}\mathbf{q}'}\Theta(k_F - \|\mathbf{k}+\mathbf{q}\|) \qquad (P) \quad (8)$$

$$\rho_{\mathbf{k}}(\mathbf{q}\sigma,\mathbf{q}'\sigma') = \frac{1}{N}\delta_{\mathbf{q}\mathbf{q}'}\delta_{\sigma\sigma'}\Theta(k_F - \|\mathbf{k}+\mathbf{q}\|) \qquad (U) \quad (9)$$

while FG energies (per electron) are in Hartree units

$$E_{FG} = \frac{3k_F^2}{10} - \frac{3k_F}{4\pi} \quad (10)$$

On the other hand, in the Wigner crystal, each $\rho_{\mathbf{k}}$ is $1/N$ times a projector of rank n_s (full band).

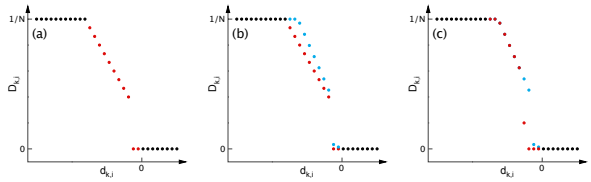

FIG. 1. Illustration of the descent algorithm for the $D_{\mathbf{k},i}$ (see III A). (a): example of a set of $D_{\mathbf{k},i}$ and $d_{\mathbf{k},i}$ with $\sum_{\mathbf{k},i} D_{\mathbf{k},i} = 1$. Red points ($D_{\mathbf{k},i} < 1/N$ and $d_{\mathbf{k},i} < 0$) can move. (b): new set $D^{(\mathrm{new})}_{\mathbf{k},i}$, see Eq.20, where blue points have moved. At this step, we have $\sum_{\mathbf{k},i} D^{(\mathrm{new})}_{\mathbf{k},i} \neq 1$ (here > 1). (c): corrected $D^{(\mathrm{new})}_{\mathbf{k},i}$, in red, in order to insure that $\sum_{\mathbf{k},i} D^{(\mathrm{new})}_{\mathbf{k},i} = 1$.

In order to describe solutions between FG and WC, we search for a lattice Λ and a density matrix $\rho_{\mathbf{k}}$ such that the number of particle per unit cell is near n_s (or some multiple of n_s for non-Bravais lattices). For extremal states, the eigenvalues of $\rho_{\mathbf{k}}$ must be exactly 0 or $1/N$, the number of strictly positive eigenvalues is not known a priori but is expected to fall between 0 and $2n_s$ (or some multiple of $2n_s$ for non-Bravais lattices).

In practice, the first M_Λ $\mathbf{q}$-vectors in Λ are used (see Table I). Thus $\rho_{\mathbf{k}}$ is a $n_s M_\Lambda \times n_s M_\Lambda$ matrix. Using the representation

$$\rho_{\mathbf{k}} = \sum_i D_{\mathbf{k},i}\,|u_{\mathbf{k},i}\rangle\langle u_{\mathbf{k},i}| \quad (11)$$

where $\langle u_{\mathbf{k},i}|u_{\mathbf{k},j}\rangle = \delta_{ij}$, the condition $0 \le \rho_{\mathbf{k}} \le 1/N$ becomes $0 \le D_{\mathbf{k},i} \le 1/N$.

Notice that each $|u_{\mathbf{k},i}\rangle$ is a Bloch wave of band index i, and can be decomposed on the $n_s M_\Lambda$ states $|\mathbf{k}+\mathbf{q};\sigma\rangle$ where $\mathbf{q} \in \Lambda$. So we note :

$$|u_{\mathbf{k},i}\rangle = \sum_{\substack{\mathbf{q}\in\Lambda\\ \sigma}} a_{\mathbf{k},i}(\mathbf{q},\sigma)\,|\mathbf{k}+\mathbf{q}\,;\sigma\rangle \quad (12)$$

where $a_{\mathbf{k},i}(\mathbf{q},\sigma)$ are the unknown complex numbers ($\propto M_\Lambda M^3$). Imposing the polarization allows us to further reduce this number.

The next subsections give details on how the parameters are found using a descent method (III A), and how the energies are efficiently computed (III B).

III. NUMERICAL DETAILS

A. Energy minimization

From Eq. (4) and Eq. (11), the energy per electron and its variation read

$$e = \sum_{\mathbf{k}\in\mathcal{B}}\sum_i D_{\mathbf{k},i}\,\langle u_{\mathbf{k},i}|\left(K_{\mathbf{k}}+\mathcal{V}_{\mathbf{k}}\right)|u_{\mathbf{k},i}\rangle \quad (13)$$

$$de = \sum_{\mathbf{k}\in\mathcal{B}} \mathbf{Tr}\, h_k^{\mathrm{HF}} d\rho_k \quad (14)$$

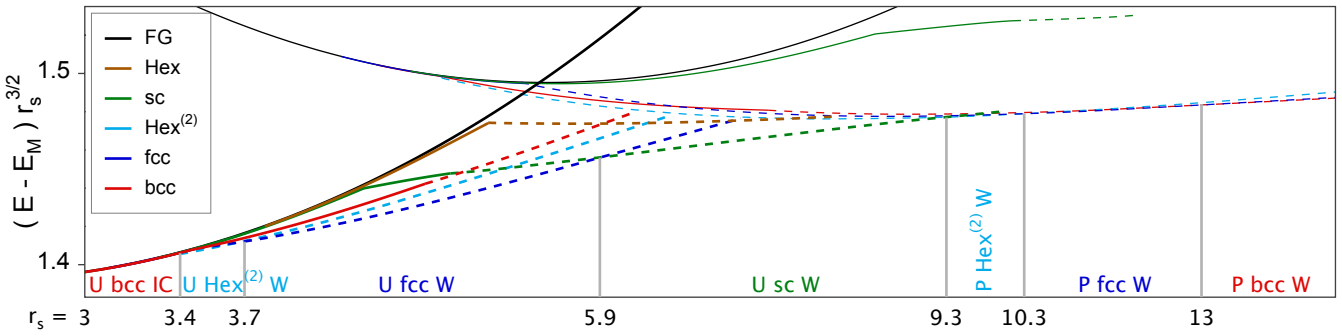

FIG. 2. Hartree-Fock phase diagram of the 3D electron gas. Energies are in Hartree per electron. $E_M = -0.89593/r_s$ is the Madelung energy of a polarized-bcc Wigner crystal. Full lines stand for incommensurate regime ($Q > Q_W$) and dashed lines for the Wigner crystal ($Q = Q_W$). Thin lines stand for the polarized gas (upper curves) and thick lines for the unpolarized gas.[14]

where

$$h^{\rm HF}_{\mathbf{k}} = K_{\mathbf{k}} + 2\mathcal{V}_{\mathbf{k}} \tag{15}$$

is the so-called HF-Hamiltonian.[3,4] From

$$\begin{aligned} d\rho_k = &|u_{\mathbf{k},i}\rangle \langle u_{\mathbf{k},i}|\, dD_{\mathbf{k},i} \\ &+ D_{\mathbf{k},i}(|du_{\mathbf{k},i}\rangle \langle u_{\mathbf{k},i}| + |u_{\mathbf{k},i}\rangle \langle du_{\mathbf{k},i}|), \end{aligned} \tag{16}$$

Eq.(14) becomes

$$de = \sum_{\mathbf{k}\in\mathcal{B}} \left[d_{\mathbf{k},i} dD_{\mathbf{k},i} + 2\Re \langle G_{\mathbf{k},i}|du_{\mathbf{k},i}\rangle\right] \tag{17}$$

with

$$G_{\mathbf{k},i} = h^{\rm HF}_{\mathbf{k}} |u_{\mathbf{k},i}\rangle \tag{18}$$

$$d_{\mathbf{k},i} = \langle u_{\mathbf{k},i}| h^{\rm HF}_{\mathbf{k}} |u_{\mathbf{k},i}\rangle . \tag{19}$$

The minimization consists in the following steps:

i) choose $D_{\mathbf{k},i}$ and $|u_{\mathbf{k},i}\rangle$ to start with,

ii) for fixed $D_{\mathbf{k},i}$, find the best $|u_{\mathbf{k},i}\rangle$ with a quadratic descent method[5],

iii) try to improve $D_{\mathbf{k},i}$ given $d_{\mathbf{k},i}$ and the linear constrains $0 \le D_{\mathbf{k},i} \le 1/N$ and $\sum_{\mathbf{k},i} D_{\mathbf{k},i} = 1$ and in case of success, go to step *ii*.

The process stops when each $D_{\mathbf{k},i}$ reaches its extrema 0 or $1/N$ with its gradient negative or positive, respectively.

Figure 1 shows how the $D_{\mathbf{k},i}$ are moved. A new set is defined as

$$D^{(\rm new)}_{\mathbf{k},i} = \max(0, \min(1/N, D_{\mathbf{k},i} - \varepsilon\, d_{\mathbf{k},i})) \tag{20}$$

$$t = \sum_{\mathbf{k},i} D^{(\rm new)}_{\mathbf{k},i} \tag{21}$$

If $t > 1$, some $D_{\mathbf{k},i}$ are decreased, those with the highest $d_{\mathbf{k},i}$ and $D_{\mathbf{k},i} > 0$, as shown in Fig.1-(c). Reversely, if $t < 1$, some $D_{\mathbf{k},i}$ are increased, those with the lowest $d_{\mathbf{k},i}$ and $D_{\mathbf{k},i} < 1/N$.

Small ε (< 0.1) ensures that the $|u_{\mathbf{k},i}\rangle$ follow the $D_{\mathbf{k},i}$ *adiabatically*. On the contrary, with large ε (~ 1), the system converge in a few steps, but the energy may end up in a local minimum. An efficient compromise is to start with $\varepsilon \sim 1$, and decrease it at each step. This allows a fast convergence to the same point as that obtained with a small ε. Except rare cases, all results are converged with 1 up to 30 moves of the $D_{\mathbf{k},i}$.

We checked on small system size ($M = 8$ or 16) that the results do not depend on the starting point. Nevertheless, the speed of convergence can be significantly improved using conditioned initial states based on the description given in Sec. IV C.

B. Implementation of $\mathcal{V}_{\mathbf{k}}$ through FFT

The largest computer time is the evaluation of $\mathcal{V}_{\mathbf{k}}$ (Eq.6). The computation of the exchange part of $\mathcal{V}_{\mathbf{k}}$ involves a convolution over the Brillouin zone $\mathcal{B}$:

$$h(\mathbf{k}_1) = \sum_{\mathbf{k}_2\in\mathcal{B}} \frac{1}{\|\mathbf{k}_1 - \mathbf{k}_2\|^2} g(\mathbf{k}_2) \tag{22}$$

Instead of computing M^3 terms ($\mathbf{k}_1$), each of them containing a sum over M^3 terms ($\mathbf{k}_2$), we would like to implement the FFT over the Brillouin zone. The main complication is that $\mathcal{B}$ is not a parallelepiped box (except in cubic case). Numerically we use the unit cell B to index the functions h and g.

$$B = \left\{ \mathbf{k} = \sum_{\alpha=1}^{3} \frac{n_\alpha}{M} \mathbf{Q}_\alpha,\ 0 \le n_\alpha < M \right\} \tag{23}$$

Any $\mathbf{k}$ in B corresponds to a unique $\hat{\mathbf{k}}$ in $\mathcal{B}$ with $\mathbf{k} - \hat{\mathbf{k}} \in \Lambda$. With this notation we have to compute:

$$h(\mathbf{k}_1) = \sum_{\mathbf{k}_2\in\mathcal{B}} f(\hat{\mathbf{k}}_1 - \hat{\mathbf{k}}_2) g(\mathbf{k}_2) \tag{24}$$

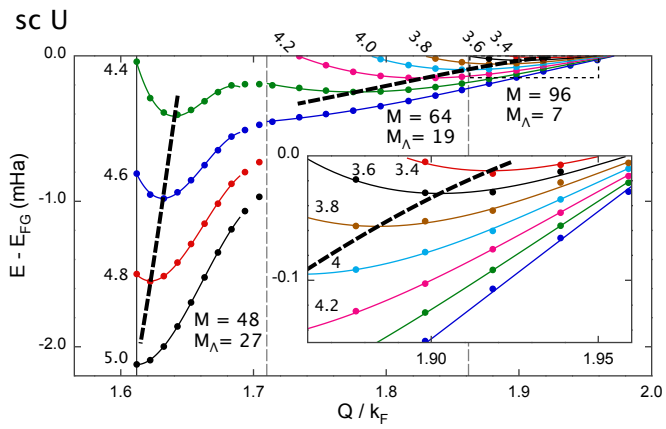

FIG. 3. Energy versus the modulation Q at various r_s for the unpolarized gas in the sc symmetry. Lines are the polynomial fits (see Eq. (32)) of the numerical results (circles). r_s is indicated at the start of each curve. Thick dashed lines fit the minima of $\mathcal{E}(r_s, Q)$ at fixed r_s. The leftmost vertical straight line stands for $Q = Q_W$. Inset: zoom of the dotted rectangle of the main figure. Gray dashed lines separate the domains of different M and M_Λ used in the numerics. The precision on the energy is always better than 10^{-5} Ha.

The function $f(\hat{k}_1 - \hat{k}_2)$, may be seen as a function on:

$$B_2 = \left\{ \mathbf{k} = \sum_{\alpha=1}^{3} \frac{n_\alpha}{M} \mathbf{Q}_\alpha,\ 0 \le n_\alpha < 2M \right\} \tag{25}$$

The dual B_2^* is the $\mathbb{Z}/2M\ \mathbb{Z}$-module generated by $\{\mathbf{L}_\alpha/2\}$. Introducing the ensemble of 8 vectors $E = \{\mathbf{e} = \sum_\alpha n_\alpha \mathbf{L}_\alpha/2,\ n_\alpha = 0 \text{ or } 1\}$, we note $B_2^* = \cup_{\mathbf{e}}(B^* + \mathbf{e})$ and B^* is $\mathbb{Z}/M\ \mathbb{Z}$-module generated by $\{\mathbf{L}_\alpha\}$. Thus we have:

$$f(\hat{\mathbf{k}}_1 - \hat{\mathbf{k}}_2) = \frac{1}{M^{3/2}} \sum_{\mathbf{e}\in E} \sum_{\mathbf{x}\in B^*} \tilde{f}_{\mathbf{e}}(x) e^{-i(\hat{\mathbf{k}}_1 - \hat{\mathbf{k}}_2)(\mathbf{x}+\mathbf{e})} \tag{26}$$

$$\tilde{f}_{\mathbf{e}}(\mathbf{x}) = \frac{1}{8M^{3/2}} \sum_{\mathbf{k}\in B_2} f(\mathbf{k}) e^{i\mathbf{k}(\mathbf{x}+\mathbf{e})} \tag{27}$$

Now we set $g_{\mathbf{e}}(\mathbf{k}) := e^{i\hat{\mathbf{k}}\mathbf{e}} g(\mathbf{k})$. Then using Eq.26:

$$f * g(\mathbf{k}_1) = \frac{1}{M^{3/2}} \sum_{\mathbf{e}\in E} \sum_{\mathbf{x}\in B^*} \tilde{f}_{\mathbf{e}}(\mathbf{x}) e^{-i\mathbf{k}_1\mathbf{x}} e^{-i\hat{\mathbf{k}}_1\mathbf{e}} \times \sum_{\mathbf{k}_2\in B} g(\mathbf{k}_2) e^{i\mathbf{k}_2\mathbf{x}} e^{i\hat{\mathbf{k}}_2\mathbf{e}} \tag{28}$$

$$= \sum_{\mathbf{e}\in E} e^{-i\hat{\mathbf{k}}_1\mathbf{e}} \sum_{\mathbf{x}\in B^*} \tilde{f}_{\mathbf{e}}(\mathbf{x}) \tilde{g}_{\mathbf{e}}(\mathbf{x}) e^{-i\mathbf{k}_1\mathbf{x}} \tag{29}$$

where

$$\tilde{g}_{\mathbf{e}}(\mathbf{x}) = \frac{1}{M^{3/2}} \sum_{\mathbf{k}\in\mathcal{B}} g_{\mathbf{e}}(\mathbf{k}_2) e^{i\mathbf{k}\mathbf{x}} \tag{30}$$

is the Fourier transform of $g_{\mathbf{e}}$.

Thus, once for all, the functions $\tilde{f}_{\mathbf{e}}(\mathbf{x})$ and $e^{i\hat{\mathbf{k}}\mathbf{e}}$ are tabulated. Thereafter, at each step, $\tilde{g}_{\mathbf{e}}(\mathbf{x})$ are computed through eight FFTs. Then the inverse FFT is applied to the eight products $\tilde{f}_{\mathbf{e}}\tilde{g}_{\mathbf{e}}$. Finally, h is obtained by summing the results with the weights $e^{-i\hat{\mathbf{k}}_1\mathbf{e}}$. Thus this procedure is of order $M^3 \ln M$ instead of M^6.

C. Size effects

In this sub-section we discuss the convergence of the results with respect to M_Λ and M.

A finite M_Λ is equivalent to a truncation of the Hilbert space (see Eq.12), thus increasing M_Λ leads to a lower energy.

At small r_s, the coefficients $a_{\mathbf{k}}(\mathbf{q})$, in Eq.12, decrease quickly with $\|\mathbf{k}+\mathbf{q}\|$. On the contrary, as r_s increases, the convergence is much slower. Fortunately, it depends very weakly on M, allowing to extrapolate to large M_Λ independently from M.

The extrapolation $M \to \infty$ corresponds to the thermodynamic limit. As shown in Ref.[9], the most important finite size effects can be written as

$$\Delta E_M \equiv E_M - E_\infty = \frac{E_1}{M} + \frac{E_2}{M^2} + \frac{E_3}{M^3} + ... \tag{31}$$

where E_1 is related to the Madelung energy, and E_2 can be evaluated from the structure factor $S(\mathbf{k})$. E_3 is non-analytical in IC but regular in WC allowing us a clean extrapolation to the thermodynamical limit.

The overall accuracy of our results depends both on M_Λ and M. At large r_s, $\rho_{\mathbf{k}}$ is smooth but extended, so M_Λ must be as large as possible but not M. At small r_s, $\rho_{\mathbf{k}}$ varies rapidly around the boundaries of the first $\mathcal{B}$, so M must be as large as possible but not M_Λ. Figure 3 shows such an optimal compromise where the error on the total energy is always smaller than 10^{-5} Ha.

IV. RESULTS

In Fig.2. we recall the phase diagram[9] displaying the geometry and polarization which yields the lowest energy at each value of r_s. At fixed geometry, for large r_s, we find a Wigner commensurate crystal (WC), as expected. As r_s decreases, an incommensurate metallic phase is found characterized by a modulation increasing from Q_W to $2k_F$ as r_s goes to 0. Such an incommensurate crystal (IC) interpolates between the WC phase and the Fermi gas. Indeed, in the reciprocal space, the momentum distribution $n(\mathbf{k})$ evolves from that of the WC phase where it is a continuous function to the Fermi gas, where $n(\mathbf{k}) = 1$ for $\|\mathbf{k}\| \le k_F$ and 0 elsewhere. In IC states, increasing pockets are build around the corners of the $\mathcal{B}$ where $n(\mathbf{k}) = 0$. Thus, in some directions $n(\mathbf{k})$ is continuous at the border of $\mathcal{B}$, as in the WC phase, whereas in other directions it is discontinuous, as in the FG at k_F. In real space, an IC-state looks like a WC

but with a larger number of lattice sites than the number of electrons. At small r_s, for unpolarized states, the IC-states present a contrast of the charge density much smaller than that of the spin density.

In the next subsection we recall how the phase diagram is obtained and we establish the universality of the results at small r_s. Subsection IV B discusses the metal-insulator transition. The subsection IV C is devoted to ground state wave function characterization. Correlations are presented in the last subsection IV D.

A. Ground state at fixed symmetry and polarization

For each lattice symmetry, we compute the ground state $e(r_s, Q)$, see for example Fig.3. Relevant values of Q lie between Q_W and $2k_F$, where Q_W is the modulation of the Wigner crystal (see Table I). At large r_s, the minimum of $e(r_s, Q)$ is at Q_W. As r_s decreases, the lowest energy may be for $Q > Q_W$. In the neighborhood of a minima, we fit $e(r_s, Q)$ with a polynomial:

$$e(r_s, Q) = \sum_{i=0}^{i_m} \sum_{j=0}^{3} a_{ij} r_s^i Q^j, \tag{32}$$

where i_m is generally 2 (and 1 when only few points are available). For fixed r_s, Q_{r_s} minimizes $e(r_s, Q)$. The thick dashed lines in Fig.3 is $e(r_s, Q_{r_s})$ as a function of Q_{r_s}. In Fig.2 are reported the dashed lines obtained for all geometries.

It is worth noticing that Q_{r_s} is always sufficiently large such that only the first band is occupied.

Fig.4 shows Q_{r_s} versus r_s. As the FG is the ground state at $r_s = 0$ and the Fermi surface is contained in $\mathcal{B}$ for $Q \geq 2k_F$, we expect that these curves should reach $2k_F$ for vanishing r_s, compatible with our results. Remarkably, at fixed polarization, Q_{r_s} slightly depends on the geometry.

This can be understood assuming SDW/CDW[11,13] holds at small r_s. A SDW is defined as a superposition of waves $|\mathbf{k}\rangle$ and $|\mathbf{k}+\mathbf{Q}\rangle$, where $\mathbf{Q}$ is a piecewise constant wave vector, such that $\mathbf{k}$ and $\mathbf{k}+\mathbf{Q}$ are close to the Fermi surface. The energy gain of the SDW's is proportional to the number of available $\mathbf{Q}$-vectors, assuming that the SDW's are independent. If the $\mathbb{Z}$-module generated by the $\mathbf{Q}$'s is discrete, then the model is actually periodic. The number $n_{\mathbf{Q}}$ of available $\mathbf{Q}$ is the number of nearest neighbors of the origin in Λ, i.e. the number of points in the first shell of Λ. Fig.5 shows that, once rescaled by $n_{\mathbf{Q}}$, these energies become very close. Whereas such a behavior may be expected at $r_s \ll 1$, it is quite remarkable that it can be applied up to $r_s \approx 3$. Further, it explains that bcc symmetry is favored as it has the largest value $n_{\mathbf{Q}} = 12$.

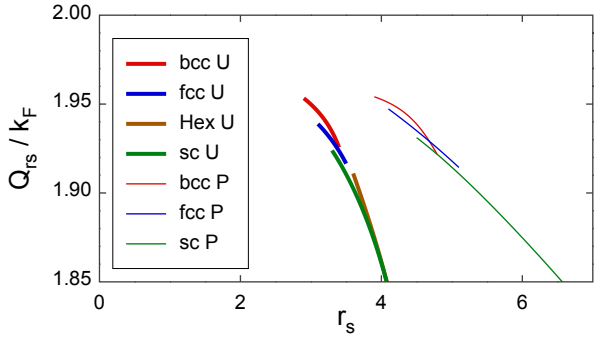

FIG. 4. Q_{r_s} per symmetry and polarization, versus r_s. Data are obtained from fits (see text : Eq.32).

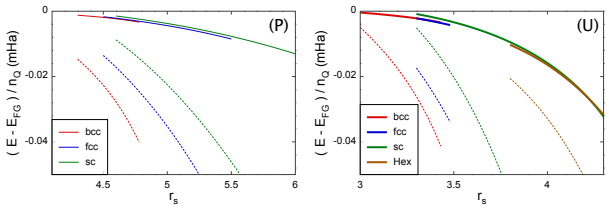

FIG. 5. Energies versus r_s of polarized (P) and unpolarized (U) IC. Dashed lines: raw energies. Full lines: energies divided by the number $n_{\mathbf{Q}}$ of available SDW's: $n_{\mathbf{Q}} = 2, 6, 8, 12$ for Hex, sc, fcc, bcc, respectively.

B. Metal-Insulator transition

From the eigenvalues of the HF Hamiltonian, Eq.15, we can plot the band structure at different densities. The band structure of the unpolarized gas in the sc symmetry for some r_s is shown in Fig.6. For *high* r_s (Fig.6-a), the solution is a WC: the first band is occupied with a finite gap corresponding to an insulator. At lower r_s (Fig.6-b,c,d), the solution becomes IC and the first band is partially occupied, corresponding to a metal. As r_s decreases, the bands approach the FG band structure. For other symmetries or polarizations, the scenarios are very similar.

Imposing $Q = Q_W$ at low r_s leads to solution with several partially occupied bands, as shown in Fig.7, and the Fermi gas can be recovered (still at $Q = Q_W$). However, when this happens, solutions with lower energies are found with $Q > Q_W$ leading to IC states.

C. Ground state wave function characterization

At fixed r_s, geometry, and polarization, only one band is occupied (see Sec.IV A). Thus, the occupied Bloch waves may be indexed by $\mathbf{k}$ and σ

$$|u_{\mathbf{k},\sigma}\rangle = \sum_{\mathbf{q}\in\Lambda} a_{\mathbf{k},\sigma}(\mathbf{q})\, |\mathbf{k}+\mathbf{q}\,;\sigma\rangle \tag{33}$$

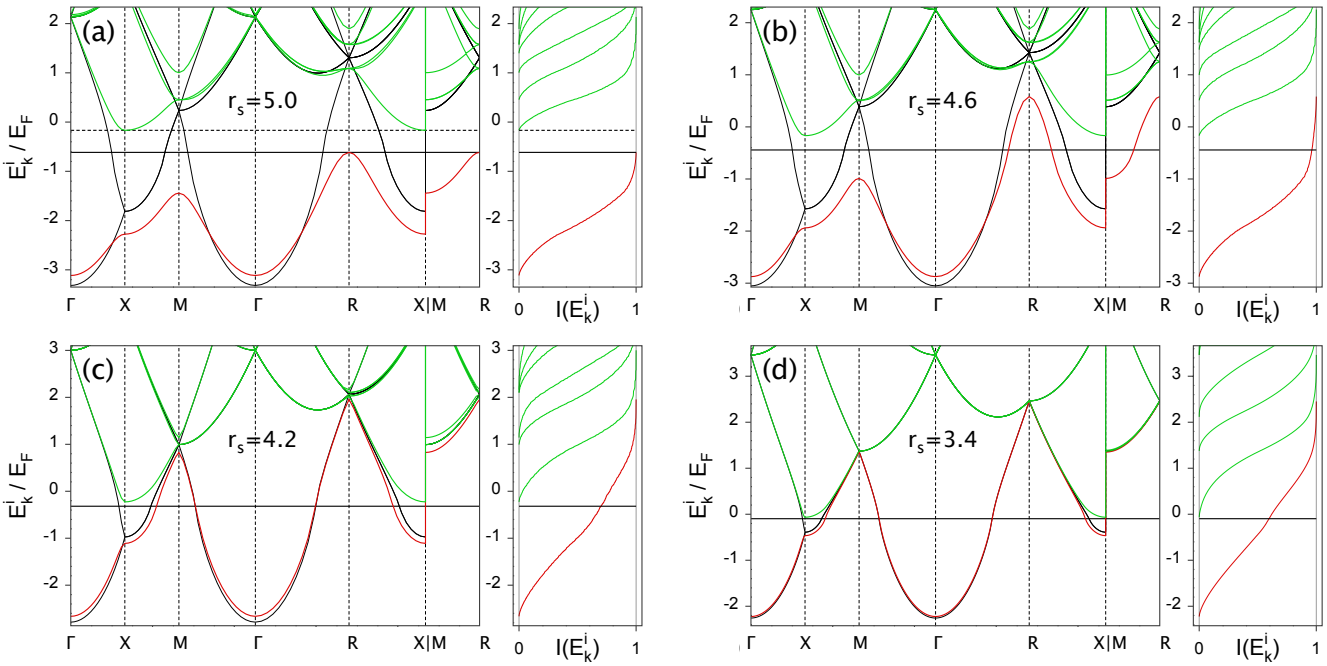

FIG. 6. HF band structure along standard path[15] (see Table I) of U sc at various density for $Q = Q_W = 1.612$ (a),1.631 (b), 1.817 (c) and 1.918 (d). Red, green and black lines stand for first band, higher bands, and FG energies, respectively. In each picture, the right plot shows the energy versus the integrated density of state of each band. The full horizontal line represents the last occupied states. In (a), the gap is the domain between this full line and the dashed line. In (b), (c) and (d), the gap vanishes.

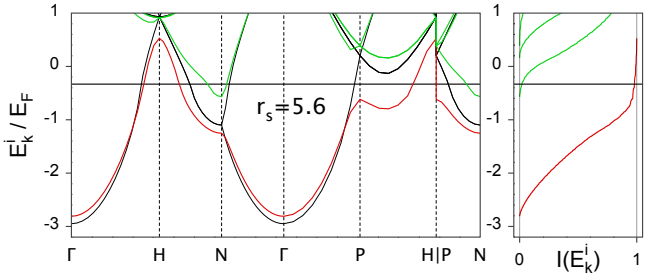

FIG. 7. Same as Fig.6 for P bcc at $Q = Q_W$ with several bands. This solution has a lower energy than WC (one band) and FG. However, at the same density a better solution is found with $Q > Q_W$.

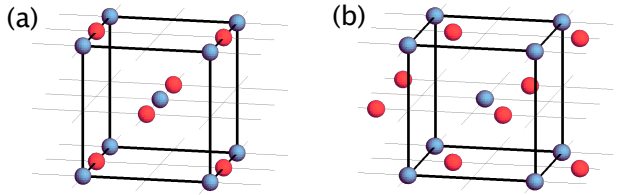

FIG. 8. U bcc real space maxima. Blue and red points stand for up and down spin density, respectively. (a) : $r_s \gtrsim 5.6$ WC states where up and down spins are *aligned*. (b) : $r_s \lesssim 5.6$ IC and WC states where up and down spins are *tilted*[16].

where $\mathbf{k}$ belongs to a subset of $\mathcal{B}$ (or exactly $\mathcal{B}$ for the WC). For P states, we find that $a_{\mathbf{k}\uparrow}(\mathbf{q})$ can be chosen real positive. For most U states, we find that spin up follow the same rule while spin down have an additional phase described by a simple translation $\mathbf{T} = (\alpha_0, \alpha_1, \alpha_2)$, in real space lattice basis, where $\alpha_i = 0$ or $1/2$: $a_{\mathbf{k}\downarrow}(\mathbf{q}) = a_{\mathbf{k}\uparrow}(\mathbf{q})e^{i\mathbf{q}.\mathbf{T}} = \pm a_{\mathbf{k}\uparrow}$. The ground states of U sc and fcc for all r_s are described by such a wave function, as well as incommensurate Hex and the WC U bcc at $r_s > 5.6$ (see Fig.8-a).

In the second family of ground states, we still have $\|a_{\mathbf{k}\uparrow}(\mathbf{q})\| = \|a_{\mathbf{k}\downarrow}(\mathbf{q})\|$. This family contains the WC with Hex symmetry and the incommensurate and WC phase with bcc symmetry at $r_s < 5.6$ (see Fig.8-b.[16])

In the Hex$^{(2)}$ case, there are two electrons per unit cell so the system occupies two bands and the amplitudes are complex numbers.

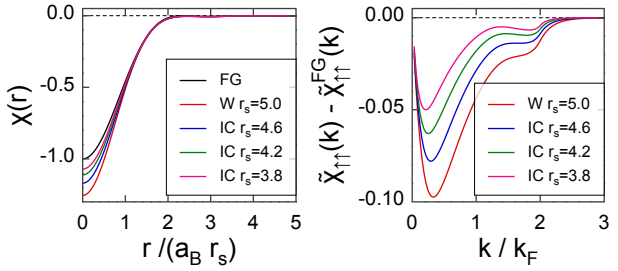

FIG. 9. Angle-averaged pair correlation function for the unpolarized gas in bcc symmetry, $\chi(r)$, see Eq. (37), and the difference between its Fourier transform $\tilde{\chi}(k)$ and $\tilde{\chi}^{\rm FG}(k)$ for $r_s = 5$, 4.8, 4.2 and 3.8 at $Q = 1.809$, 1.818, 1.827 and 1.836 respectively. At smaller values of r_s, inside the IC phase with $Q > 1.9$, the difference to the FG is less than 10^{-2}.

D. Correlation functions

We define the 1-body density ρ_1 as:

$$\rho_1(\mathbf{r},\sigma;\mathbf{r}',\sigma') = \sum_{\mathbf{k},\mathbf{k}'} \rho_1(\mathbf{k},\sigma;\mathbf{k}',\sigma') e^{i(\mathbf{k}\mathbf{r}-\mathbf{k}'\mathbf{r}')} = \sum_{\substack{\mathbf{k}\in\mathcal{B}\\ \mathbf{q}',\mathbf{q}'\in\Lambda}} \rho_{\mathbf{k}}(\mathbf{q},\sigma;\mathbf{q}',\sigma') e^{i\mathbf{k}(\mathbf{r}-\mathbf{r}')} e^{i(\mathbf{q}\mathbf{r}-\mathbf{q}'\mathbf{r}')} \quad (34)$$

We consider the two-body correlation function, using the same notation of Eq.(2)

$$\chi(\underline{1},\underline{2};\underline{1}',\underline{2}') = \rho_2(\underline{1},\underline{2};\underline{1}',\underline{2}') - \rho_1(\underline{1};\underline{1}')\rho_1(\underline{2};\underline{2}') \quad (35)$$

From the HF factorization of the two-body density matrix, Eq. 2, we obtain the correlation function χ, defined such that $\chi = 0$ when the correlations vanish:

$$\chi_{\sigma,\sigma'}(\mathbf{r},\mathbf{r}') = -\rho_1(\mathbf{r},\sigma;\mathbf{r}',\sigma')\rho_1(\mathbf{r}',\sigma';\mathbf{r},\sigma) \quad (36)$$

and, concerning the average distance of a pair,

$$\chi_{\sigma,\sigma'}(\mathbf{r}) = \lim_{V\to\infty} \frac{1}{V} \int d\mathbf{r}'\, \chi_{\sigma,\sigma'}(\mathbf{r}'+\mathbf{r},\mathbf{r}') = -\sum_{\mathbf{q}\in\Lambda} \left| \sum_{\substack{\mathbf{k}\in\mathcal{B}\\ \mathbf{q}'\in\Lambda}} \rho_{\mathbf{k}}(\mathbf{q}',\sigma;\mathbf{q}'-\mathbf{q},\sigma') e^{i(\mathbf{k}+\mathbf{q})\mathbf{r}} \right|^2 \quad (37)$$

and its Fourier transform is denoted $\tilde{\chi}_{\sigma,\sigma'}(\mathbf{k})$. For unpolarized systems, we have $\chi_{\uparrow\uparrow} = \chi_{\downarrow\downarrow}$ and $\chi_{\uparrow\downarrow} = 0$.

Figure 9 shows the comparison of the HF-correlation functions with the Fermi gas solution, $\chi^{FG}_{\uparrow\uparrow}(r) = -9\left[\sin(x) - x\cos(x)\right]^2/x^6$ with $x = k_F r$ and $\tilde{\chi}^{FG}_{\uparrow\uparrow}(k) = 3q/4 - q^3/16$ with $q = k/k_F < 2$ and $\tilde{\chi}^{FG}_{\uparrow\uparrow}(k) = 0$ for $k > 2k_F$. As one can see, the pair correlations change smoothly between different phases and remain close the FG.

V. CONCLUSION

In this paper we have presented our numerical algorithm which has been used to obtain the HF phase diagram presented in Ref.[9], and discussed various properties of the solutions, focusing on the IC phase. Here, we have given evidence that the IC states are very close to pure spin or charge density wave superimposed in different directions, so that the structure proposed by Overhauser[11] in 1962 is essentially recovered. From the band structure, we expect these states to have metallic character very close to the usual FG and also similar pair correlations.[16]

Is the spin density ground state stable against the inclusion of correlations beyond the Hartree-Fock approximation? In the high density region, correlation energies[17] largely exceeds the HF energy difference between spin or charge density waves and the homogeneous FG. Nevertheless, since these broken symmetry states only introduce tiny modifications in the very proximity of the spherical Fermi surface of the FG, correlations will shift their energies by almost the same amount as the FG. Assuming a rigid shift in the correlation energy, our calculations indicate the possibility of spin or charge density waves at rather low temperatures. In real materials, they will then be in competition to other instabilities, e.g. superconductivity.

[1] N.F. Mott, Proc. Phys. Soc. A **62**, 416 (1949).
[2] S. Huotari, J. A. Soininen, T. Pylkkänen, K. Hämäläinen, A. Issolah, A. Titov, J. McMinis, J. Kim, K. Esler, D. M. Ceperley, M. Holzmann, and V. Olevano, Phys. Rev. Lett. **105**, 086403 (2010).
[3] N.W. Ashcroft and N.D. Mermin, Solid State Physics, Saunders, Philadelphia (1976).
[4] G. F. Giuliani and G. Vignale, *Quantum Theory of the Electron Liquid*, Cambridge University Press, Cambridge (2005).
[5] B. Bernu, F. Delyon, M. Duneau, and M. Holzmann, Phys. Rev. B 78, 245110 (2008); cond-mat/0810.3559.
[6] B. Bernu, F. Delyon, M. Holzmann and L. Baguet, Phys. Rev. **B 84**, 115115 (2011); cond-mat/0810.3559.
[7] J. R. Trail, M. D. Towler, and R. J. Needs, Phys. Rev. **B 68**, 045107 (2003).
[8] S. Zhang and D. M. Ceperley, Phys. Rev. Lett. **100**, 236404 (2008), arXiv:0712.1194 (2007).
[9] L. Baguet, F. Delyon, B. Bernu, and M. Holzmann, Phys. Rev. Lett. **111**, 166402 (2013)

symmetry	sc	bcc	fcc	Hex	Hex$^{(2)}$
n_c	1	1	1	1	2
M_Q	$\begin{pmatrix} 1 & 0 & 0 \\ 0 & 1 & 0 \\ 0 & 0 & 1 \end{pmatrix}$	$\frac{1}{\sqrt{2}}\begin{pmatrix} 0 & 1 & 1 \\ 1 & 0 & 1 \\ 1 & 1 & 0 \end{pmatrix}$	$\frac{1}{\sqrt{3}}\begin{pmatrix} -1 & 1 & 1 \\ 1 & -1 & 1 \\ 1 & 1 & -1 \end{pmatrix}$	$\frac{4\sqrt{2}}{3}\begin{pmatrix} 1 & -0.5 & 0 \\ 0 & \sqrt{3}/2 & 0 \\ 0 & 0 & 3/(4\sqrt{2}) \end{pmatrix}$	
γ^3	1	$\frac{1}{\sqrt{2}}$	$\frac{4}{3\sqrt{3}}$	$\frac{16}{3\sqrt{3}}$	
Q_W/k_F	1.611991954016	1.809399790564	1.758882522024	1.108026556895	0.879441261012
d^2	$n_1^2+n_2^2+n_3^2$	$d_{sc}^2+n_1n_2+n_1n_3+n_2n_3$	$d_{sc}^2-\frac{2}{3}(n_1n_2+n_1n_3+n_2n_3)$	$\frac{32}{9}(n_1^2+n_2^2-n_1n_2)+n_3^2$	
M_Λ	7 , 19 , **27** , 33 , 57	13 , **19** , 43 , 55 , 79	9 , **15** , 27 , 51 , 59	3 , 9 , 11 , **23** , 35	
C_Λ	-2.837297479481	-2.888461503054	-2.888282119020	-2.512880623796	
S-P	Γ : (0 0 0) X : ($\frac{1}{2}$ 0 0) M : ($\frac{1}{2}$ $\frac{1}{2}$ 0) R : ($\frac{1}{2}$ $\frac{1}{2}$ $\frac{1}{2}$)	Γ : (0 0 0) N : ($\frac{1}{2}$ 0 0) H : ($\frac{1}{2}$ $\frac{1}{2}$ $-\frac{1}{2}$) P : ($\frac{1}{4}$ $\frac{1}{4}$ $\frac{1}{4}$)	Γ : (0 0 0) X : ($\frac{1}{2}$ $\frac{1}{2}$ 0) W : ($\frac{1}{2}$ $\frac{3}{4}$ $\frac{1}{4}$) K : ($\frac{3}{8}$ $\frac{3}{4}$ $\frac{3}{8}$) L : ($\frac{1}{2}$ $\frac{1}{2}$ $\frac{1}{2}$) U : ($\frac{5}{8}$ $\frac{5}{8}$ $\frac{1}{4}$)	Γ : (0 0 0) M : ($\frac{1}{2}$ 0 0) K : ($\frac{2}{3}$ $\frac{1}{3}$ 0) A : (0 0 $\frac{1}{2}$) L : ($\frac{1}{2}$ 0 $\frac{1}{2}$) H : ($\frac{2}{3}$ $\frac{1}{3}$ $\frac{1}{2}$)	

TABLE I. Lattice definitions and properties. n_c is the number of sites per primitive cell. Matrix M_Q is defined by $M_Q = (\mathbf{Q}_1/Q, \mathbf{Q}_2/Q, \mathbf{Q}_3/Q)$ where $\mathbf{Q}_i$ are normalized reciprocal lattice vectors in cartesian coordinates. For the hexagonal case, $Q = ||\mathbf{Q}_3||$. $\gamma^3 Q^3$ is the volume of $\mathcal{B}$. $Q_W/k_F = \gamma(4\pi/(3n_c))^{1/3}$. d^2 is the square distance in the basis $\mathbf{Q}_i$. M_Λ's values are the numbers of vectors with integer coordinates in the first shells. Bold values indicate the minimum of M_Λ for which a neighborhood of $\mathcal{B}$ is covered. C_Λ is the Madelung constant. S-P are symmetry points of $\mathcal{B}$[15], given in reciprocal lattice vectors coordinates.

[10] E. P. Wigner, Trans. Faraday Soc. **34**, 678 (1938); Phys. Rev. **46**, 1002 (1934).

[11] A. W. Overhauser, Phys. Rev. Lett. **4**, 462 (1960); Phys. Rev. **128**, 1437 (1962).

[12] A. J. Coleman: Rev. Mod. Phys., **35**, 668 (1963),

[13] F. G. Eich, S. Kurth, C. R. Proetto, S. Sharma, and E. K. U. Gross, Phys. Rev **B 81**, 024430 (2010)

[14] Excepted a narrow range of density we have also shown that imposing the polarization either polarized (P) or unpolarized (U) with $N_\uparrow = N_\downarrow$ does not change the results (see supplementary material of ref[9]).

[15] W. Setyawan, S. Curtarolo, Comp. Mat. Sci. **49** (2010) 299

[16] Additional figures, tables and row data are available at http://www.lptmc.jussieu.fr/lptmcdata/3DEG/HF/

[17] D. M. Ceperley and B. J. Alder, Phys. Rev. Lett. **45**, 566 (1980).